The Astrophysical Journal, 770:64 (13pp), 2013 June 10 doi:10.1088/0004-637X/770/1/64

THE IMACS CLUSTER BUILDING SURVEY. IV. THE LOG-NORMAL STAR FORMATION HISTORY OF GALAXIES

Michael D. Gladders[1], Augustus Oemler[2], Alan Dressler[2], Bianca Poggianti[3], Benedetta Vulcani[3], and Louis Abramson[1,4]
[1] The Department of Astronomy and Astrophysics, and the Kavli Institute for Cosmological Physics, The University of Chicago, 5640 South Ellis Avenue, Chicago, IL 60637, USA; gladders@oddjob.uchicago.edu
[2] The Observatories of the Carnegie Institution of Science, 813 Santa Barbara Street, Pasadena, CA 91101, USA
[3] INAF-Osservatorio Astronomico di Padova, vicolo dell'Osservatorio 5, I-35122 Padova, Italy
Received 2012 August 10; accepted 2013 March 29; published 2013 May 24

ABSTRACT

We present here a simple model for the star formation history (SFH) of galaxies that is successful in describing both the star formation rate density (SFRD) over cosmic time, as well as the distribution of specific star formation rates (sSFRs) of galaxies at the current epoch, and the evolution of this quantity in galaxy populations to a redshift of $z = 1$. We show first that the cosmic SFRD is remarkably well described by a simple log-normal in time. We next postulate that this functional form for the ensemble is also a reasonable description for the SFHs of individual galaxies. Using the measured sSFRs for galaxies at $z \sim 0$ from Paper III in this series, we then construct a realization of a universe populated by such galaxies in which the parameters of the log-normal SFH of each galaxy are adjusted to match the sSFRs at $z \sim 0$ as well as fitting, in ensemble, the cosmic SFRD from $z = 0$ to $z = 8$. This model predicts, with striking fidelity, the distribution of sSFRs in mass-limited galaxy samples to $z = 1$; this match is not achieved by other models with a different functional form for the SFHs of individual galaxies, but with the same number of degrees of freedom, suggesting that the log-normal form is well matched to the likely actual histories of individual galaxies. We also impose the sSFR versus mass distributions at higher redshifts from Paper III as constraints on the model, and show that, as previously suggested, some galaxies in the field, particularly low mass galaxies, are quite young at intermediate redshifts. As emphasized in Paper III, starbursts are insufficient to explain the enhanced sSFRs in intermediate redshift galaxies; we show here that a model using only smoothly varying log-normal SFHs for galaxies, which allows for some fraction of the population to have peak star formation at late times, does however fully explain the observations. Finally, we show that this model, constrained in detail only at redshifts $z < 1$, also produces the main sequence of star-formation observed at $1.5 < z < 2.5$, again suggesting that the log-normal SFHs are a close approximation to the actual histories of typical galaxies.

Key words: galaxies: evolution – galaxies: formation – galaxies: statistics

Online-only material: color figures

1. INTRODUCTION

Simple analytic models for the star formation histories (SFHs) of galaxies have been explored for decades, and a number of basic SFHs have found common usage in a variety of analyses. These SFHs range from utilitarian models such as continuous star formation or true simple stellar populations (i.e., a delta-function burst), through to more complex histories such as truncated continuous star formation (Larson & Tinsley 1978), exponentially declining star formation (Searle et al. 1973), and the delayed exponential SFH (e.g., Gavazzi et al. 2002) as first proposed by Sandage (1986).

Of course, all such simple models of entire galaxies are considered to be time-averaged representations of a multitude of star formation events occurring in individual star forming regions on timescales much smaller than the dynamical timescale of a typical galaxy. In detail the SFH of a galaxy is almost certainly not easily described by a simple function, but rather as the accumulation of a large number of brief star formation episodes associated to some extent with the merger history of that galaxy and its parent dark matter halo. An appreciation of the importance of the effect of secondary bursts on various observables has been present in the literature for decades (cf. Larson & Tinsley 1978); secondary bursts are particularly critical when predicting the observed properties of early type galaxies, where bursts involving only a few percent of the galaxies total stellar mass can significantly alter some spectroscopic and photometric observables (e.g., Kaviraj et al. 2009).

Paper III of this series (Oemler et al. 2013b) presents a detailed look at the measured star formation rates in field galaxy populations from $z = 0$ to $z = 1$, and notes in particular that the observed evolution of the specific star formation rate (sSFR; the star formation rate per unit stellar mass) cannot be explained by simple models in which galaxies are coeval populations, and furthermore that starbursts cannot modify the sSFR distribution in such a model to match the observed values. The data suggest that some galaxies must form the bulk of their stars reasonably quickly at late times, from which we conclude that any successful analytic model for the SFHs of individual galaxies must control both the onset time and timescale of star formation; single parameter models such as exponentially declining SFHs are insufficient.

In this paper we present a treatment of galaxy SFHs in which we use a fit to the cosmic star formation rate density (SFRD) as the basis for a functional form for the SFH of typical galaxies. The SFRD is a measure of star formation as a function of lookback time and as such *is* the SFH of the hypothetical average

[4] Current address: Brinson Fellow at the Observatories of the Carnegie Institution of Science, 813 Santa Barbara Street, Pasadena, CA 91101, USA.

galaxy. We explore the ability of aggregate populations of this simple SFH to match fundamental observables such as the local and intermediate redshift distribution of sSFRs in galaxies. The sSFR distribution encodes the mass (i.e., the integrated SFH) and the current star formation rate, and the relationship between these. We motivate the functional form of the SFH—simply a log-normal in time—in Section 2, and provide simple fits to the data from Paper III using only the SFRD and the $z = 0$ sSFR distribution.

In Section 3 we attempt to connect a suite of log-normal histories to individual galaxies and add additional constraints from the measured sSFR distribution of galaxies out to $z = 1$. In Section 4 we discuss the implications of this modeling in the context of the conclusions of Paper III, noting that this model successfully produces some young galaxies at late times without starbursts. In Section 5 we discuss the broader implications of the apparent efficacy of the log-normal SFHs. We summarize our main results and suggest some future tests of this model in Section 6.

2. THE LOG-NORMAL SFH

The ubiquity of the log-normal distribution in nature is well known (e.g., Limpert et al. 2001). Skewed distributions such as this will arise with physical processes where negative values are not permitted. Star formation, like many other "growth" processes, is such a process; negative values of star formation do not occur. It is thus reasonable to suppose that the SFH of a typical galaxy might appear log-normal. Further, the history of star formation in the universe—the SFRD—is strongly skewed in time (e.g., Bouwens et al. 2009) and is at least reminiscent of a log-normal distribution, with a rapid rise at early times, and long slow decline at late times. The log-normal distribution is also a two-parameter function, and so at least in principle can provide sufficient flexibility to match the sSFR evolution highlighted in Paper III. This fact, the shape of the SFRD, and the apparent ubiquity of log-normal distributions in nature motivates the current analysis.

2.1. The Log-normal Cosmic Star Formation Rate Density

Current data (see, for example, the compilation in Cucciati et al. 2012) clearly show both a rise and fall in the SFRD over cosmic time. More specifically, the rise in the SFRD is fast at early times, with a long continuing but declining tail of star formation to the present epoch. Ignoring mergers, the shape of the SFRD should represent the shape of the SFH of the mean galaxy in the universe. Of course, the actual SFH of any recognized single galaxy at $z = 0$ will likely not fit this description, not least because a typical $z = 0$ galaxy is thought to represent the merger of a number of smaller systems over cosmic time.

Putting aside this complexity for the moment, we note that the presence of both a rise and fall in the SFRD also indicates that simple SFH models which decline from initially high star formation rates (i.e., exponentially declining models—referred to as τ models—commonly used in modeling the spectrophotometric properties of galaxies at later times) cannot easily describe the overall SFRD evolution; a delay time *must* be allowed—such as in the delayed exponential SFH of Sandage (1986)—in order to even approximate current data. The rise in the SFRD from high redshift can be produced by an ensemble of simple τ models if a second parameter—the time at which such a SFH "turns on"—is allowed and is appropriately distributed at early times.

Recent analysis of the photometric properties of distant galaxies also argues for a SFH *in individual galaxies* that is smoothly rising at early times (Maraston et al. 2010). They found that an SFH of SFR $= Ae^{-(t-t_o)/\tau}$, a so-called inverted-τ model, produced a better fit to the photometric properties of a sample of $z \sim 2$ actively star forming galaxies than did the more typically used declining-τ models. A similar result, for galaxies with a fixed comoving number density of 2×10^{-4} Mpc^{-3}, was found to hold from $z = 8$ z to $z = 3$ by Papovich et al. (2011); Reddy et al. (2012) find that rising SFHs at $7 > z > 2$ are the preferred history for a sample of galaxies observed at $z \sim 2$. Maraston et al. also note that the results of Cimatti et al. (2008) from a study of $z \sim 1.6$ elliptical galaxies also argue for an early SFH that is rising in time. Additionally, some studies suggest that the sSFR of galaxies is flat beyond the peak of the SFRD at $z \sim 2$ out to at least $z \sim 7$ (e.g., Stark et al. 2009; González et al. 2010), though see de Barros et al. (2012) for an alternate view; one simple interpretation of such a flattening is that individual galaxies at these redshifts have SFHs with a star formation rate smoothly increasing to later times. This overall picture of rising SFHs in individual galaxies at high redshift is also found in recent cosmological hydrodynamic simulations (Finlator et al. 2011; Jaacks et al. 2012).

Maraston et al. point out that the remarkably ubiquitous use of declining τ models in the literature over the past few decades is not well justified, and has become thoroughly divorced from the original aim of these models of measuring the age of early-type galaxies at $z \sim 0$. It thus seems reasonable to seek a new simple model which captures both the rising early-time and declining late-time behavior of galaxy SFHs.

In seeking a functional form to describe the SFRD over cosmic time, we have explored a number of possible descriptions, and have found that a remarkably simple one—a log-normal in time—works extremely well. We describe the scale free log-normal distribution of the star formation rate as

$$\mathrm{SFR}(t, t_0, \tau) = \frac{1}{t\sqrt{2\pi\tau^2}} e^{-\frac{(\ln t - t_0)^2}{2\tau^2}}, \quad (1)$$

where t is the elapsed time since the big bang, t_0 is the logarithmic delay time, and τ sets the rise and decay timescale. One great advantage of such a form over some other models—such as the inverted-τ model of Maraston et al. (2010) is that it naturally subsumes both a rising and falling SFH at different times; simple τ models—inverted or otherwise—are aphysical, whereas a log-normal in time could arguably describe the SFH of a galaxy (or at least a galaxy's components) at all times. A further advantage is that the delay time is de-coupled from the width of the SFH, unlike the delayed exponential model of Sandage (1986). Behroozi et al. (2013) have recently suggested two other functional forms—a double power law, or a hybrid exponential+powerlaw—which we will explore further below.

Figure 1 shows a fit to the SFRD with a single log-normal. This simple functional form produces an reasonable fit, with a χ^2 of 2.1. It is worth re-emphasizing that the log-normal, besides providing an good fit, is a functional form that emerges again and again in the analysis of distributions in natural systems. From the failure rate of electronic components (Salemi et al. 2008) to the latency periods of infectious diseases (Kondo 1977) and many other systems, the log-normal distribution appears as the preferred rate model. Log-normal distributions occur when multiplicative effects dominate; that the cosmic SFRD is log-normal in time suggests a deeper meaning than that it is simply a good fit.

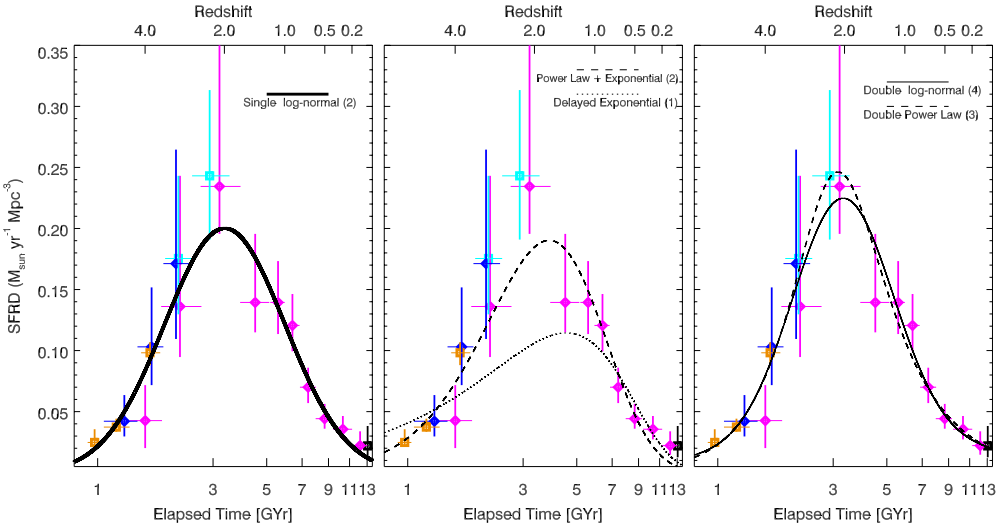

Figure 1. SFRD measurements are from the literature, as compiled in Cucciati et al. (2012), plotted vs. elapsed time. Magenta diamonds are the measurements of Cucciati et al. (2012); orange squares are from Bouwens et al. (2009), blue diamonds from van der Burg et al. (2010), cyan squares from Reddy & Steidel (2009), and the single low-z measurement in black is from Wyder et al. (2005). Uncertainties are as reported in Cucciati et al. (2012); horizontal lines indicate the redshift range over which each measurement was made. The left panel shows the best fit log-normal ($t_0 = 1.539$; $\tau = 0.574$); this simple form appears to be an apt description of the cosmic SFRD. The center panel shows the best fits using two SFH models from the literature—the power-law+exponential from Behroozi et al. (2013) and the delayed exponential (Gavazzi et al. 2002)—neither of which is a good fit to the data. The right panel shows the fit achieved with two more complex models—the double power-law from Behroozi et al. (2013) and a double log-normal ($t_0 = 1.394, 2.803$; $\tau = 0.459, 1.187$). In all panels the number of shape parameters in each fitting function is indicated parenthetically.

(A color version of this figure is available in the online journal.)

Figure 1 also shows fits to several other functional forms suggested in the literature:

1. the best fitting delayed exponential SFH, given by the SFH $\propto t/\tau^2 \exp(-t^2/2\tau^2)$; the fit is obviously poor—with a χ^2 of 10.2. This result is not unexpected, given the coupling of delay time and width in this model with a single shape parameter;
2. the best fitting exponential + power-law (Behroozi et al. 2013), given by SFH $\propto t^A \exp(-t/\tau)$; this model, with the same number of parameters as the single log-normal, produces a poorer fit, with a χ^2 of 4.3;
3. the best fitting double power-law (Behroozi et al. 2013), given by SFH $\propto ((t/\tau)^A + (t/\tau)^{-B})^{-1}$; this three-parameter model fits the distribution extremely well, with a χ^2 of 1.7.

The apparent agreement between different datasets seen in Figure 1 suggests that the uncertainties on the data as reported are overestimated—or include a significant correlated systematic component. We caution that a reduced χ^2 is thus not trivial to compute; however the relative χ^2 of models with the same number of parameters—i.e., the single log-normal and the exponential + power-law is still informative. In this comparison the log-normal is clearly preferred.

Figure 1 also shows the result of a double log-normal fit (where each log-normal component has equal weight). This fit resolves any lingering tension between the peak height and late-time SFRD present in the single log-normal fit. The χ^2 of this fit is 1.6. We include the double log-normal fit here primarily because it yields an interesting physical interpretation; one of the fitted SFHs is characterized as an early onset with a fast decline and the other as a somewhat later onset with a slower decline. These two basic SFHs could be interpreted as corresponding to early- and late-type galaxies, or even the bulge and disk components of the typical galaxy. We also use the double log-normal fit as a smooth description of the cosmic SFRD.

The simple model fits above have been computed using a downhill simplex, but in general in this paper we fit ensembles of parameterized SFH models to data using a simulated annealing algorithm; the choice of simulated annealing to thoroughly explore the parameter space for large aggregate samples of SFHs will become apparent in the next section.

2.2. The Specific Star Formation Rate at $z = 0$

The $z = 0$ sSFR of a given galaxy is the current star formation rate divided by total mass, and the total mass is the integral of the SFH for that galaxy, adjusted for stellar mass loss. The $z = 0$ sSFR distribution is thus a reasonably orthogonal measure to the SFRD over cosmic time, and a potentially useful constraint on a SFH model. We illustrate this point in Figure 2, which shows the τ, t_0 parameter plane for a log-normal SFH, with lines of constant $z = 0$ sSFR and lines of constant time of peak star formation shown. The displayed range of sSFRs brackets values seen in several samples of galaxies discussed below. Over much of that range, lines of constant sSFR and lines of constant peak time are approximately orthogonal—i.e., imposing both a history and a current sSFR selects one particular curve for most galaxies. Only galaxies with large sSFRs at the present epoch are poorly constrained in this way.

As discussed in Paper III, an evolution in the rate of starbursts in galaxies is insufficient to explain the observed evolution in the sSFR distributions from low to high redshift. The presence of a main sequence of star formation at both low and high redshifts has led numerous authors (e.g., Noeske et al. 2007; Rodighiero et al. 2011) to conclude that starbursts are subdominant in affecting the observed evolution in star formation in galaxies, as is also seen in simulations (Di Matteo et al. 2008). While it is apparent that secondary starbursts do happen, our aim in this paper is to explore the ability—or lack thereof—of smooth SFH models to reproduce the observed trends in sSFR, completely absent any starbursts.

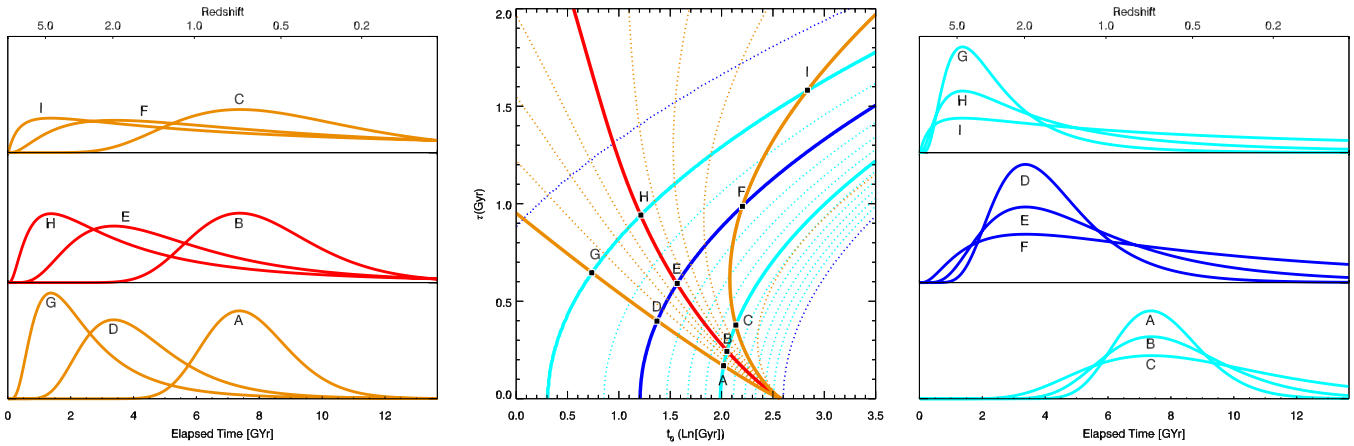

Figure 2. Center panel: lines of constant $z = 0$ sSFR (red, orange) and constant time of peak star formation (blue, cyan) in the τ, t_0 parameter plane. Constant sSFR lines are shown at 5%, 15%, ..., 95% of the non-zero sSFR rates in the dataset described later in Section 2.2. Galaxies with no measured star formation will appear to the bottom left of this figure. Blue lines show the location of τ, t_0 parameter values for redshifts of 10.5, 2.0 and 0.0 (the nominal epoch of reionization from the *Wilkinson Microwave Anisotropy Probe* (Larson et al. 2011), the peak of the cosmic SFRD, and the present, respectively), with cyan lines spaced by 1 Gyr centered earlier and later than $z = 2.0$. Secondary panels: individual log-normal SFHs are shown along the heavier lines in the main panel, at the intersections of the heavy lines as picked out by black point and labeled both in the main panel and in secondary panels; panels to the right show log-normal distributions along lines of constant time of peak star formation (for example, the middle of these three panels, colored blue, shows SHFs which peak at $z = 2$, along the heavy blue line in the main panel) and panels to the left show log-normal distributions along lines of constant $z = 0$ sSFR (for example, the middle of these three panels, colored red, shows SHFs with a fixed $z = 0$ sSFR along the heavy red line in the main panel). All secondary panels are scaled to the same arbitrary peak SFR.

(A color version of this figure is available in the online journal.)

Motivated by Figure 2, we consider the $z \sim 0$ sSFR distribution for galaxies, for which we use the local galaxy sample described in Paper III. Two sub-samples are included. The first, taken from the PG2MC survey (Calvi et al. 2011), covers a larger volume, but has a higher mass limit of $4 \times 10^{10}\ M_{\odot}$, with minimum and maximum redshifts of 0.03 and 0.11 and a median redshift of 0.0918. The second, from the Sloan Digital Sky Survey (SDSS) observations of the northern galactic cap, is more restricted in redshift, with minimum and maximum redshifts of 0.035 and 0.045 and a median redshift of 0.0401. This second sub-sample has a lower mass limit of $1 \times 10^{10}\ M_{\odot}$, and is cut at the upper end at the lower limit of the first sub-sample. Galaxies are weighted to bring the two sub-samples to a common volume. As described in Oemler et al. (2013a; Paper I of this sequence) masses for this second sub-sample have been computed using a variant of the technique in Bell & de Jong (2001) with delayed exponential models (see Section 2.1) as the underlying form of the SFH.

The total sample is 2094 galaxies, distributed in sSFR versus mass as shown in Figure 3, with a mean weighted redshift of 0.0678. The sSFR values are computed from Hα fluxes. The detectability of star formation depends on Hα equivalent widths and as a result the sSFR limit is not trivial to describe, as it relies both on the flux of the Hα line in emission, as well as the continuum strength, including the depth of the Hα line in absorption. The resulting incompleteness does not appear exactly fixed in either star formation rate (this would be the expected result if only the Hα line flux were relevant, for example) or sSFR (which would be expected if only the Hα equivalent width were relevant). Figure 3 also shows the fraction of galaxies which are measured as having a sSFR identically zero as a function of mass; as expected early-type systems with no measurable Hα emission are proportionately more common at the high mass end. For the purposes of this paper, we estimate the threshold sSFR—i.e., the allowed upper limit of the actual value of the sSFR for a galaxy of a given mass measured in the data in Paper III to have sSFR = 0—as simply a fixed star formation rate of $0.05\ M_{\odot}\ \mathrm{yr}^{-1}$. Note that the exact choice of limits does not significantly affect any of the results which follow.

To create a sample of SFHs that match both the $z \sim 0$ sSFR distribution and the cosmic SFRD, we proceed as follows. We consider a simulated sample of 2094 galaxies with masses identical to the sSFR data discussed above. The SFH for each galaxy is described by two parameters, τ and t_0. We jointly solve for these parameters for each galaxy in the ensemble using simulated annealing, requiring at the same time that the mass- and sample-weighted sum of the individual SFHs match the shape of the double log-normal model fit to the cosmic SFRD as detailed in Figures 1 and 2. We do not use the raw SFRD data detailed in Figure 1, but the smooth fit to these data, since this modeling process produces an under-constrained realization rather than a unique best-fit model. Galaxies with a sSFR measured to be zero in the data are allowed to take any value up to the mass-dependent threshold shown in Figure 3.

The sSFR value for each simulated galaxy at its measured redshift is computed simply as the ratio of the star formation rate divided by the mass, where the latter is the integral of the former from early times to the time of observation, modified downward by stellar mass loss that occurs over the galaxy's history. We take the functional form of this mass loss from Jungwiert et al. (2001) and as in Maraston et al. (2010) scale the mass loss so that the total loss at 10 Gyr is 40%. We do not attempt to compute the mass loss individually for each galaxy, convolved across its SFH; rather, for computational simplicity and efficiency we simply compute the mass loss from the peak of the SFRD at $z \sim 2$ to the epoch of observation for each galaxy. The differences between this approach and a more refined computation are in general small because much of the mass loss that occurs at early times, and by $z \sim 0$ the bulk of the star formation in galaxies is well in the past.

The resulting distribution of sSFR values, and the distribution of τ and t_0 parameters, is shown in Figure 4. The fit is reasonable; however, Figure 4 reveals a certain amount of tension between the SFRD constraints and the $z = 0$ sSFR constraints when fitting each galaxy with a log-normal SFH. Specifically, the

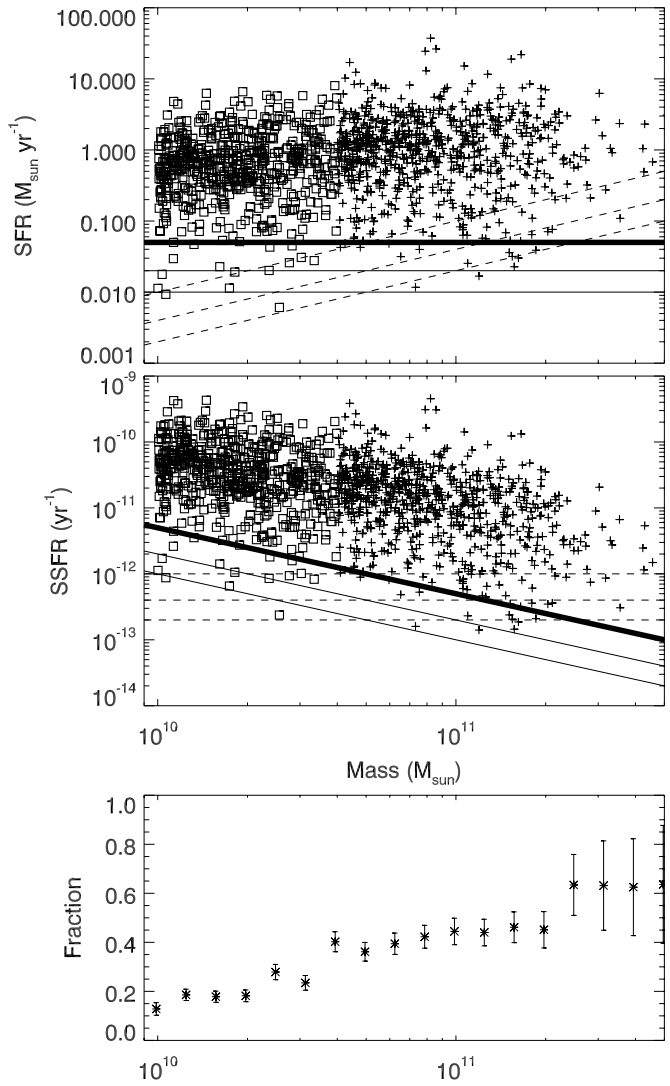

Figure 3. The top two panels show the distribution of star formation rates (top) and sSFRs (middle) vs. mass at $z \sim 0$ for the $z \sim 0$ data from Paper III. Objects reported as having an sSFR identically equal to zero are not shown. The data are drawn from two regions with differing volumes, and hence objects have differing relative weights in the combined sample (indicated by different symbols). Dashed lines are lines of constant sSFR (very approximately these are lines of constant Hα equivalent width) at limits of 2×10^{-13}, 4×10^{-13}, and 1×10^{-12} yr^{-1}. Solid lines are lines of constant star formation rate (effectively lines of constant Hα flux) at limits of 0.01, 0.02, and 0.05 $M_\odot$ yr^{-1}. The thicker solid line indicates the adopted threshold for galaxies with sSFRs identically equal to zero, as discussed in the main text. The bottom panel shows the fraction of these galaxies as a function of mass, in logarithmically spaced bins.

SFRD shape prefers a somewhat higher normalization of the $z = 0$ sSFR distribution than the actual measurements suggest. This is apparent in the fit shown in Figure 4 in two ways: (1) the final fitted values of the sSFR for each galaxy are on average slightly high, and (2) the galaxies with sSFRs that are nominally zero in the data are fit with sSFR values that pile up at the adopted upper threshold for the allowed sSFR values.

The source of this tension is, effectively, the mass limitation of the input $z \sim 0$ dataset, coupled to the changing contribution of galaxies of various luminosities to the cosmic SFRD as a function of redshift. Cucciati et al. (2012) explore the contribution of galaxies of varying far-ultraviolet luminosities and find that fainter galaxies contribute more significantly at lower redshifts. This is the expected result from an overall downsizing in the star formation in galaxies, with more massive (and generally more luminous) galaxies forming their stars earlier, as first noted by Cowie et al. (1996). The consequence of this effect in our analysis is that the contribution of the least massive and faintest galaxies that are not included in our $z \sim 0$ sample varies as a function of redshift, and hence the nominal shape of the cosmic SFRD as reported in Cucciati et al. (2012) is not completely appropriate to the particular set of $z \sim 0$ galaxies we are considering here.

However, we might reasonably expect that any subset of galaxies drawn from the overall population would itself have a cosmic SFRD that is also well described by a log-normal function in time. Indeed the SFRDs in Cucciati et al. (2012) decomposed by luminosity appear to make a homologous set. Figure 5 demonstrates a model very similar to Figure 4, except that we have allowed for an additional log-normal component designed to mimic the contribution of the faintest galaxies to the cosmic SFRD. We include this as a component whose mass is set at 5×10^9 $M_\odot$ (a factor of two below the lower mass threshold of the data) and with an sSFR set from the mean mass–sSFR relation apparent in Figure 3. The total weight of this component (i.e., equivalent to setting the number of such galaxies) is such that it produces 20% of the total star formation in the SRFD diagram. This extra component—designed to mimic the contribution of the faintest and least massive galaxies—is fit as part of the modeling and behaves exactly as expected; i.e., interpreted as individual galaxies these are somewhat later-forming systems with a peak of star formation at $z = 1.0$, which contributes most significantly to the SFRD at $z = 0$. This component is shown in Figure 5. The addition of this component resolves the tension in the model noted above.

Finally, note that measured precisely from the model in Figure 5 at the weighted mean redshift of the input sSFR sample, this component produces 43% of the star formation at that redshift. Figure 6 shows the mass-sorted cumulative star formation in the input data, as well as the nominal asymptote that this additional component suggests. This extra amount of star formation appears perfectly reasonable. Note that this agreement is at least somewhat arbitrary, as our choice of weight for this extra component does affect (and was informed by) Figure 6.

3. COMPARISON TO SPECIFIC STAR FORMATION RATES TO $z = 1$

3.1. An Unconstrained Model to $z = 1$

That the realization of a galaxy population described above matches both the SFRD as well as the $z \sim 0$ sSFR distribution does not in itself clearly validate the choice of a log-normal SFH for individual galaxies. For example, one could in principle assemble the SFRD from a large ensemble of galaxies and from a large range of functional forms (simple tophat or Gaussian SFHs, for example), and one can imagine that at least some of these may very well reproduce both the SFRD and the $z \sim 0$ sSFR distributions.

To provide some insight on this point, we next compare the results of the above log-normal realization to the data from Paper III on galaxy populations at intermediate redshifts; specifically we compare the predicted sSFR distributions to the measured values. In this first analysis we simply compare the predictions of the model to that data; a model using the higher-z data as a constraint is presented in Section 3.2. Data are drawn from two sources, as described in Paper III: the field sample from the IMACS Cluster Building Survey (ICBS), and the

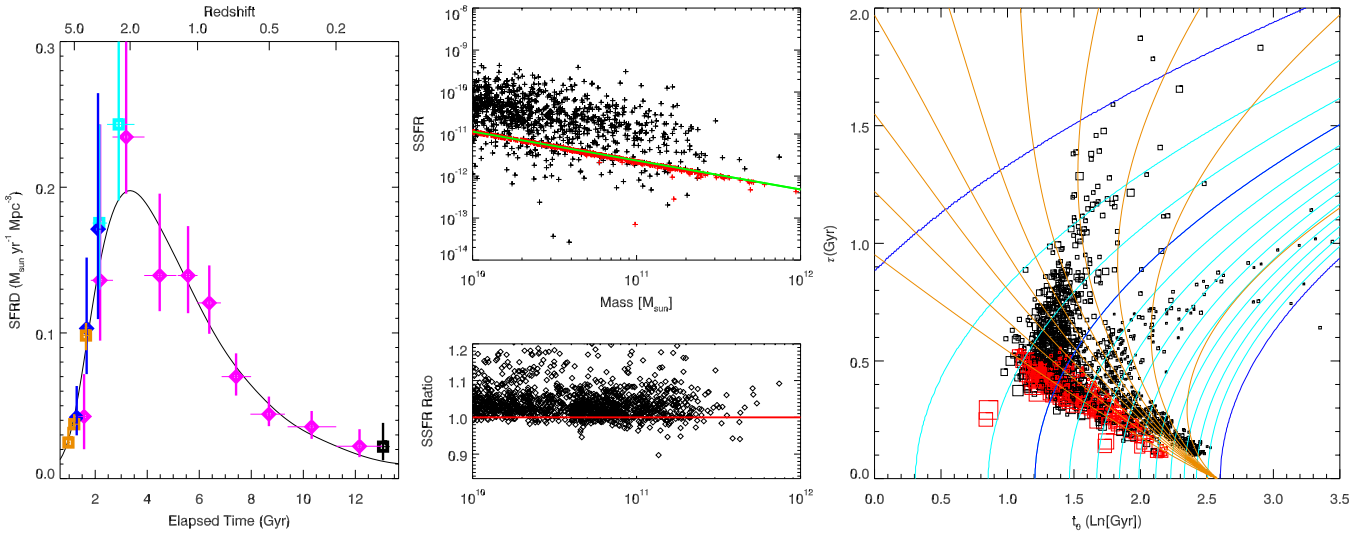

Figure 4. Left panel: the fit to the cosmic SFRD from a model realization which jointly fits these data as well as the $z \sim 0$ sSFR distribution. Data, symbols, and colors are as in Figure 1. Center panel, top: the corresponding fitted sSFR values for galaxies with a measured non-zero sSFR (black) and those which are reported with an sSFR of exactly zero (red). The allowed maximum value of the sSFR for these nominally non-star-forming galaxies, described in Figure 3, is shown by the green line. This model realization does not include any allowance for missing low-mass but high-sSFR galaxies; note the pile-up of nominally non-star-forming systems (the red symbols along a single line) at the upper limit. Center panel, bottom: the ratio of the fitted sSFR values to the measured sSFR values for the black points (galaxies with measured non-zero sSFR) in the upper panel; again note the tendency toward higher sSFRs in the model. Right panel: the distribution of log-normal parameters t_0 and τ. Symbols are individual galaxies with colors having the same meaning as the top center panel, and symbol size is proportional to the galaxy mass. The lines are as in Figure 2, though simplified.

(A color version of this figure is available in the online journal.)

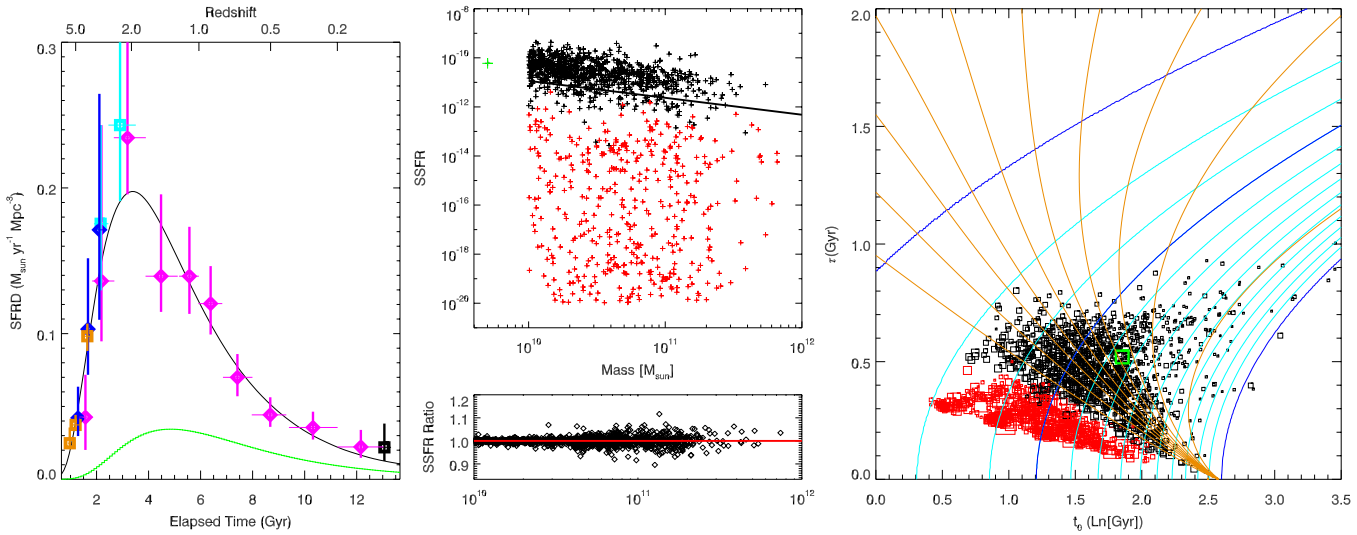

Figure 5. Similar to Figure 4, except for the addition of a single extra log-normal component which accounts for the low-mass but high-sSFR galaxies not present in the $z \sim 0$ sSFR data, and which effectively resolves the tension between the cosmic SFRD and the $z \sim 0$ data.

(A color version of this figure is available in the online journal.)

All-wavelength Extended Groth Strip International Survey (AEGIS; Davis et al. 2007). SFRs in the ICBS are computed from a hierarchy of methods calibrated against 24 μm fluxes, with Hα used where available, then Hβ, or [O II] λ3727 when not. 24 μm fluxes are used for the brightest such objects (see Paper I and III for further details). As described in Paper III, the SFRs in the AEGIS sample have been recalibrated to our measurements and our calibration by reconsidering their 24 μm fluxes and also measuring and calibrating emission lines in a set of DEEP2 spectra (upon which the AEGIS sample is based) using our own tools. All SFRs at all redshift are thus measured, as best possible, on the same calibrated system.

We compare the model predictions to data in four redshift bins: $0.2 < z < 0.4$ and $0.4 < z < 0.6$ from the ICBS field galaxy sample, and $0.6 < z < 0.8$ and $0.8 < z < 1.0$ from AEGIS. The mass limits, the approximate sSFR limits for 100% completeness, the total number of galaxies, and the fraction above the sSFR 100% completeness limit in each redshift bin are given in Table 1. Masses for the ICBS samples are as described in Paper I, computed in a manner akin to Bell & de Jong (2001) but with delayed exponential SFHs as the underlying star formation model. Masses for the AEGIS subsamples are taken from Davis et al. (2007) but converted to a Saltpeter initial mass function to match the other samples.

Before comparing the log-normal modeled sSFR distributions to the galaxy data two further corrections are necessary. First, note that the modeling as constructed does not explicitly account for merging; the individual SFHs tagged to individual galaxies

Table 1
Field Galaxy Data at Intermediate Redshifts

Sample	Redshift Range	Mass Limit ($M_\odot$)	sSFR Limit (yr^{-1})	No. of Galaxies	Fraction Above sSFR Limit
ICBS	$0.2 < z < 0.4$	1×10^{10}	2×10^{-11}	466	0.534
ICBS	$0.4 < z < 0.6$	4×10^{10}	4×10^{-11}	296	0.405
AEGIS	$0.6 < z < 0.8$	1×10^{10}	6×10^{-11}	843	0.604
AEGIS	$0.8 < z < 1.0$	2×10^{10}	5×10^{-11}	706	0.704

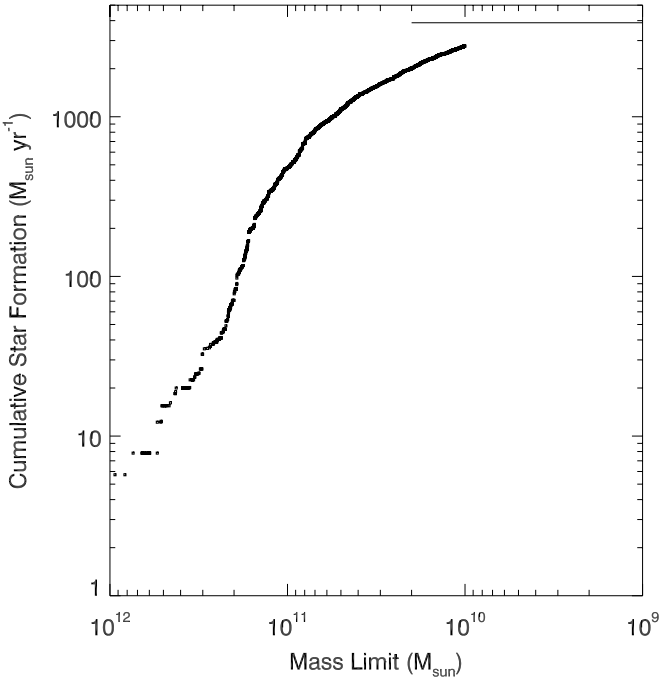

Figure 6. The cumulative total star formation in the $z \sim 0$ galaxy sample, down to a given mass limit. At the lower mass limit it is clear that not all of the local star formation is accounted for. The horizontal line shows the implied total star formation in the sample including the missing component included in the extra low-mass log-normal component shown in detail in Figure 5; this total is a reasonable asymptote given the measured data.

at $z \sim 0$ must be unmerged as one goes to higher redshift, since local galaxies are built up, to some extent, from smaller components over cosmic time. We will compare the model realization to the actual data by integrating the model over mass down to the appropriate mass limit, so a simple treatment of the merger history of the model galaxies is sufficient. Specifically we wish to know whether any individual galaxy in the $z \sim 0$ sample remains above the mass limit in a higher redshift sample, or has "un-merged" and one or more of its un-merged components have been removed from the higher redshift sample by virtue of now falling individually below the mass limit. We draw a description of the mass-dependent rate for major mergers from Xu et al. (2012) and from this compute the merger rate over redshift for each $z \sim 0$ galaxy from the present epoch back to a redshift assigned at random from the redshifts measured in the higher redshift bin. There are no strong trends in mass or sSFR versus redshift in these higher redshift datasets, so this simple process should adequately model the higher redshift data, and intra-bin variations in merger rates and sSFRs, without overly complicating this computation of a best-fit realization. Using this merger rate from Xu et al. we construct many realizations of the merger history of each galaxy, allowing for mergers, if they occur, with mass ratios up to a 3:1 split, and allowing mergers up to two steps deep in the merger tree for each $z \sim 0$ galaxy. From this ensemble of mock histories we compute the likelihood that each $z \sim 0$ galaxy (or a portion thereof) remains in the sample in the higher redshift bin when cut at the appropriate mass limit, and use these likelihoods as weights when computing the final sSFR distributions for the model. Note the correction due to accounting for merging in this way is not dramatic; in the highest redshift bin the variation in weights across the entire mass range is less than a factor of two.

The second correction is straightforward; when assessing a given SFH at higher redshifts (closer in time to the peak of the star formation in a given galaxy) somewhat less stellar mass has been lost. We adjust the galaxy masses and sSFRs appropriately.

Figure 7 shows the comparison of the sSFR distributions measured from the data reported in Table 1 and for the model realization shown in Figure 5. Modeled galaxies are assessed at the same redshift in the higher redshift bin used to compute the merger histories. The agreement is remarkably good. That the overall scaling matches—i.e., that the model tracks the movement of the sSFR distributions to higher values at earlier times—is not in itself surprising, as this is implicit in the fact that the model matches the cosmic SFRD. However, the fact that the shapes of the distributions at sSFRs higher than the 100% completeness limit agree rather well with the measured distributions—in all four redshift bins, comprising some 60% of the total timeline of star formation in the universe—is striking. The agreement is not perfect—for example in the highest redshift bin the model somewhat overpredicts the abundance of the highest sSFR galaxies—but nevertheless it suggests quite strongly that the choice of a log-normal SFH for each galaxy is well motivated. This agreement need not have happened; it is not explicit in the modeling process, as we will explore further in Section 5 below.

3.2. A Constrained Model to $z = 1$

The next step in our analysis is to create a model realization that uses the higher redshift sSFR data as an explicit constraint, in addition to the $z \sim 0$ sSFRs. In this realization we retain the mass distribution given by the $z \sim 0$ galaxies. An explicit galaxy-by-galaxy comparison to the higher redshift data is not possible, since the different datasets described in Paper III sample different co-moving volumes to different mass and sSFR limits in each redshift bin, and moreover a methodology to account in detail for the merging of galaxies across redshift bins—beyond the simple calculation sketched above—is not apparent. Thus any constraint must, to some extent, integrate across mass to ameliorate differences in the galaxy mass functions between the various datasets, and then compare distributions of sSFR values or related quantities, rather than making a galaxy-by-galaxy comparison. Indeed the comparison of model outputs to sSFR distributions in Section 3.1 does exactly that, integrating across mass directly, down to the mass limit of each redshift bin, and then simply comparing histograms

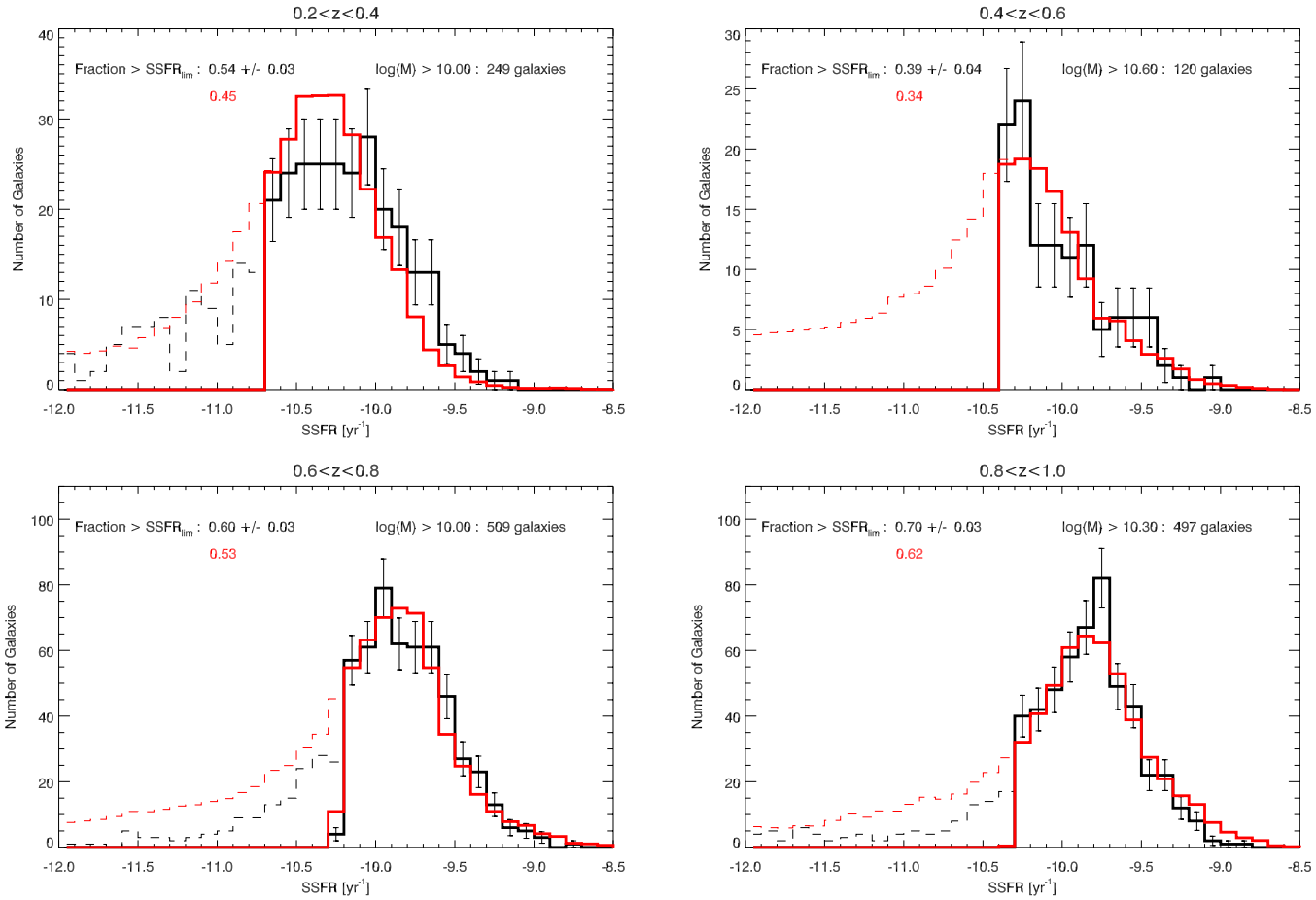

Figure 7. The comparison between the measured sSFR distribution (black) and the model prediction (red) for the model realization shown in detail in Figure 5, in four distinct redshift bins. Mass limits for each redshift range are as indicated. Thick lines show the sSFR range thought to be complete; thin dashed lines show the region that is incomplete. Many of the measured galaxies in this latter region have sSFRs which are nominally zero, and so do not contribute to these plots. The fraction of galaxies above the fiducial completeness sSFR is shown in each panel for both the measured galaxies and the model realization. Uncertainties reported on the data are simple 1σ counting errors. Given the somewhat arbitrary details of the treatment of the galaxies with sSFRs nominally zero, and the uncertainty in the actual sSFR completeness value, we anticipate that the actual uncertainty on the reported fractions is a factor of several times higher than reported and likely dominated by systematic effects. For example, modifying the sSFR completeness limits by on the order of 10% produces a change comparable to the quoted random uncertainty. Overall the fit between the data and the model prediction is remarkably good.

(A color version of this figure is available in the online journal.)

of the logarithm of the sSFRs. This is likely not an optimal approach for constraining the model, however.

A closer look at the sSFR versus mass distribution for each redshift bin of the data, shown in Figure 8, illustrates the model-to-data comparison we have chosen to impose as a constraint on the model. Specifically, note that the sSFR versus mass values form a linear sequence in log–log space: this is the star-formation main sequence described by many authors at many redshifts (see Rodighiero et al. 2011 for a recent summary). This sequence appears to have an approximately constant width with mass. Over the redshift interval considered here, there is also no strong evidence for an evolution in the slope of this linear sequence; the zeropoint clearly evolves to higher values of sSFR at higher redshift but the slope remains approximately constant. To construct a distribution of sSFR-like values to constrain the model we thus consider the cumulative distribution of the difference between log(sSFR) at various redshifts and this relation at $z = 0$, over the appropriate mass range in each redshift bin. The resulting cumulative distributions for the data are given in Figure 8.

As in Section 3.1 above, the effect of mergers is computed as a weight for each $z \sim 0$ galaxy, and appropriately used when computing the cumulative distribution of residual sSFRs in the model. This final realization of the model, now additionally using the sSFR data in the higher redshift bins as a constraint, is shown in Figure 9.

We remind the reader that all galaxies in these final model realizations have only smooth SFHs described by log-normal functions. No starburst activity is included. Starbursts might induce rapid—albeit temporary—changes in a given galaxy's sSFR, and we might expect to see this reflected as a tension between the sSFR distributions at low and high redshift, when attempting to connect the low and high redshift datasets using a smoothly varying SFH. However, the model in Figure 9 successfully incorporates all of the sSFR distributions to $z = 1$ without including any starbursts, a point discussed at length in the next section.

4. THE STAR FORMATION HISTORIES OF GALAXIES TO $z = 1$ AND BEYOND

In Paper III we highlighted several important aspects of the SFH of galaxies required by the redshift evolution of the sSFR distribution of intermediate redshift galaxies. In particular, Paper III illustrates that even at these intermediate redshifts some galaxies must be surprisingly young, having formed the bulk of

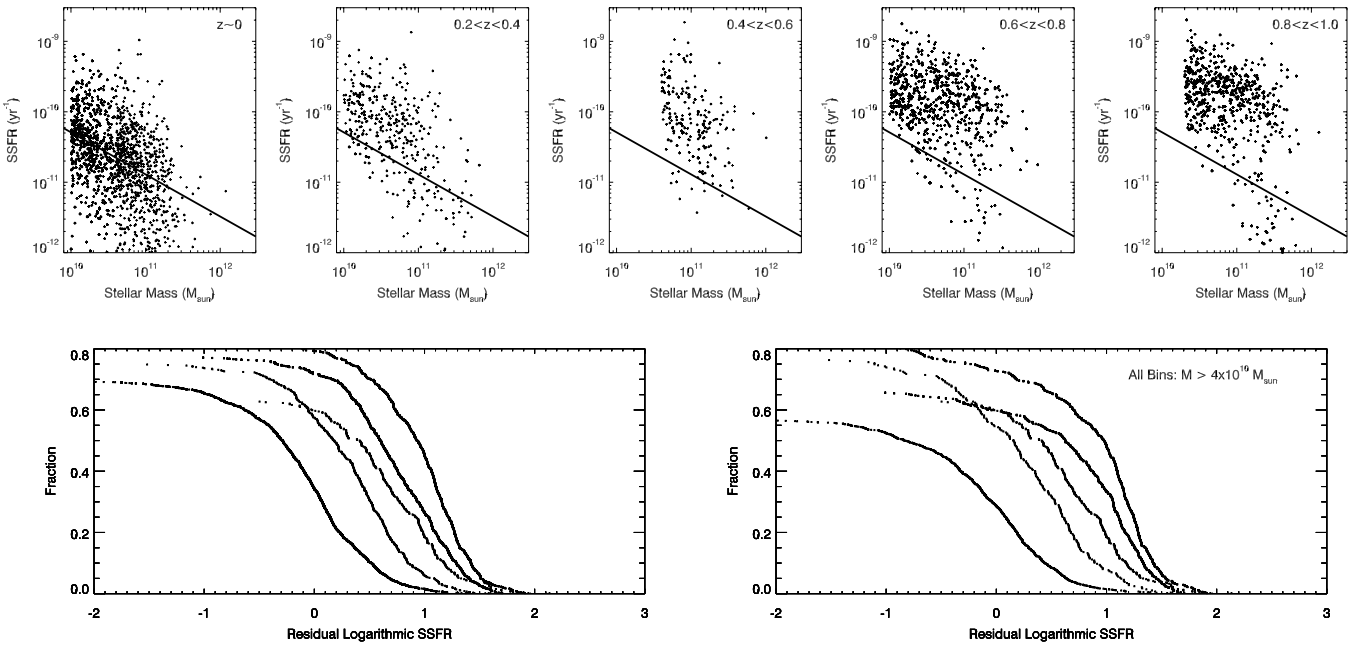

Figure 8. Top panels: sSFR vs. mass for the data summarized in Table 1; redshift bins increase in redshift to the right from the $z \sim 0$ sample on the left. The solid line shows the nominal $z \sim 0$ star formation main sequence, fit using these data, and reproduced in the other panels for comparison. The two bottom panels show residual distributions of log(sSFR) minus this trend, computed to the limiting mass of each redshift bin (left panel) or to a common limit of $4 \times 10^{10}\ M_{\odot}$ (right panel). The distributions on the bottom left are taken as constraints on the final model, down to the estimated completeness limit in sSFR in each redshift bin. Below this limit, the cumulative fraction in the fitted model is required to be at least as large as the measured (incomplete) fraction.

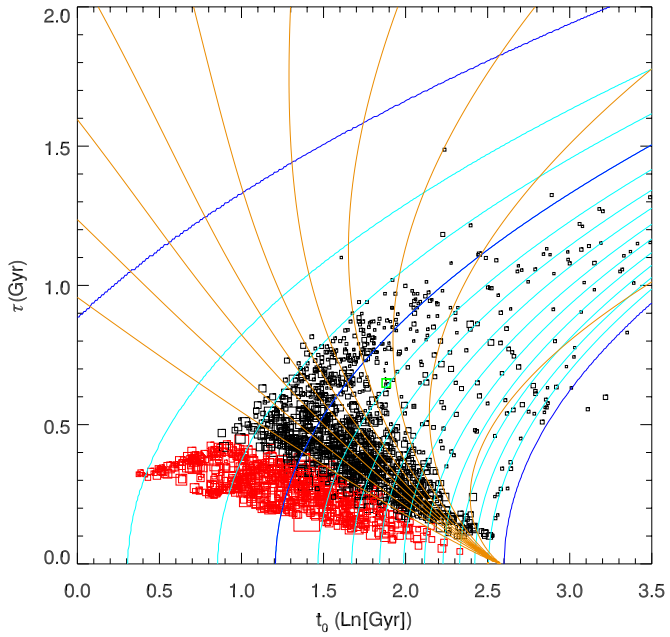

Figure 9. The distribution of t_0 and τ parameters for the final model realization, using the cumulative sSFR residuals as in Figure 8 as constraints. Colors and symbols are as in Figures 4 and 5.

(A color version of this figure is available in the online journal.)

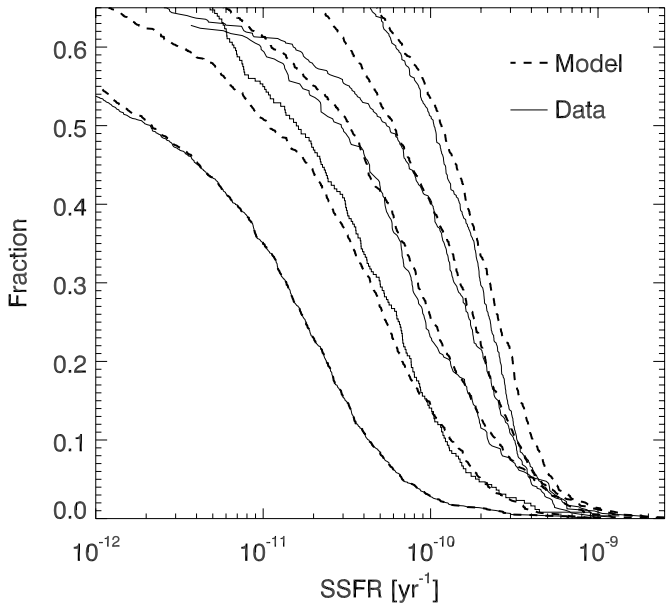

Figure 10. The cumulative sSFR distribution for all five redshift intervals considered, limited to $M \geqslant 4 \times 10^{10}\ M_{\odot}$ as in Figure 4 of Paper III. Thin solid lines show the distributions from the data; heavier dashed lines are the results from the final model realization discussed in Section 3.2. Redshift increases from left to right.

their stellar populations in their recent past, and moreover that starbursts, or a change in the prevalence thereof, cannot explain the enhancement of sSFR values seen toward higher redshifts. The final model realization above provides some further insight into the age distribution.

First, consider Figure 10, which shows the cumulative sSFR fraction in each redshift bin in the model, akin to Figure 4 in Paper III. Note that the model does an excellent job of reproducing the main trends seen in the data. This model has no starbursts, yet can reproduce the observed data with great fidelity. This provides a companion datum to previous statements regarding starbursts; not only can starbursts not readily produce the observed evolution, we show here that a population of galaxies with SFHs that have *only* a smooth component in time can in principle produce the measured sSFR distributions. This does not argue that starbursts do not change

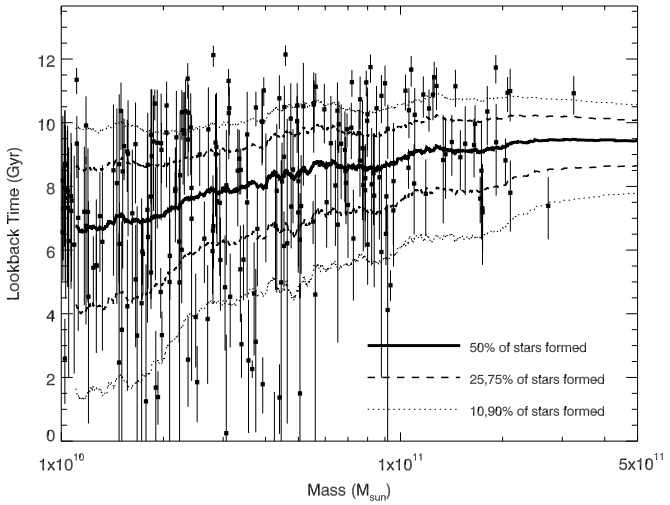

Figure 11. The lookback time at which each modeled galaxy has completed 50% of its star formation (heavy symbols), for the final model using the higher redshift sSFR distributions as a constraint, against galaxy mass at $z \sim 0$. Only some galaxies are plotted, for clarity. Vertical lines show the time interval over which each galaxy forms 10% to 90% of its stars. Overplotted curves show the typical value of the 10% and 90% times (thin dotted lines), the 25% and 75% times (heavier dashed lines), and the 50% time (heavy solid line). These typical values are computed as the mean in a running window across mass, 150 galaxies wide. Note that unlike most other times discussed elsewhere in this paper, this figure uses lookback time from $z = 0$.

the observed distributions of sSFR—they clearly must do so, for a small subset of all galaxies observed at any epoch. However, the broad trends in sSFR over a Hubble time can be reproduced completely absent a starbursting component.

Figure 11 shows the modeled ages of galaxies across galaxy mass. Note that, as suggested in Paper III, some galaxies are indeed young overall, having formed only half their stars within the past few Gyr. Moreover there is a general trend toward lower masses for more star formation at later times; the mean lookback time for galaxies at $2 \times 10^{11}\ M_{\odot}$ to have formed half their stars is about ∼9 Gyr ago, with 90% of the star formation typically completed by ∼7 Gyr ago, whereas for a $2 \times 10^{10}\ M_{\odot}$ galaxy these numbers are ∼7 and ∼2 Gyr ago, respectively.

5. THE SIGNIFICANCE OF THE LOG-NORMAL SFH

The ubiquity of log-normal distributions in nature, and the apparently excellent fit of the log-normal distribution to the cosmic SFRD, and its utility even as a description of the SFH of individual galaxies, leads unavoidably to speculation on whether this distribution is somehow special in the context of star formation, or more simply provides a reasonable fit because it has the required basic properties; i.e., it rises at early times, falls at later times, and provides a two-parameter family of curves with both a duration and onset of star formation that are independent (unlike, for example, a delayed exponential in

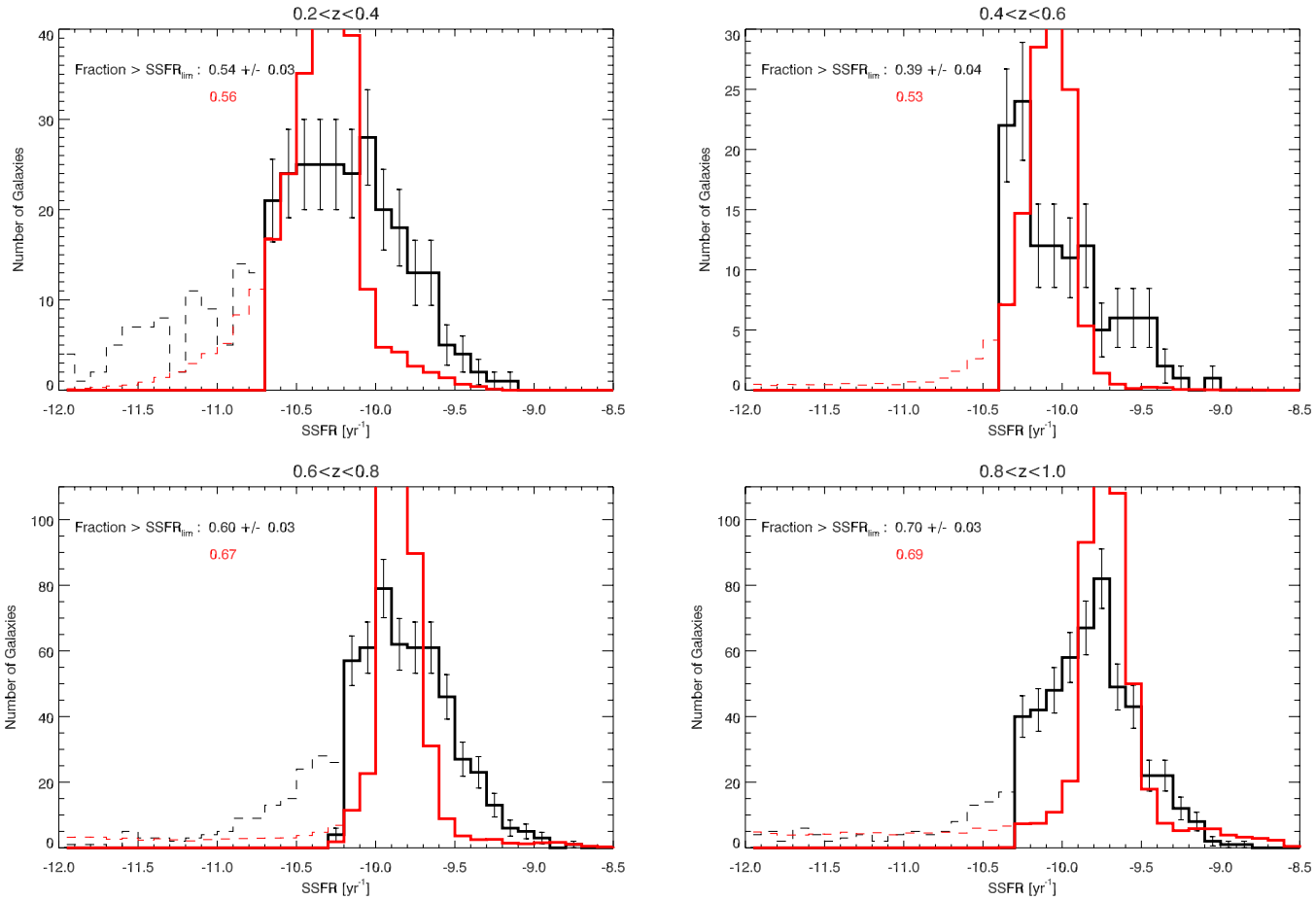

Figure 12. As Figure 7, except that the model used has Gaussian SHFs for galaxies rather than log-normal SFHs. The model is constrained by the $z \sim 0$ sSFR distribution and the cosmic SFRD as for the model shown in Figures 5 and 7. The higher redshift predictions for this model are poor by comparison to the log-normal model.

(A color version of this figure is available in the online journal.)

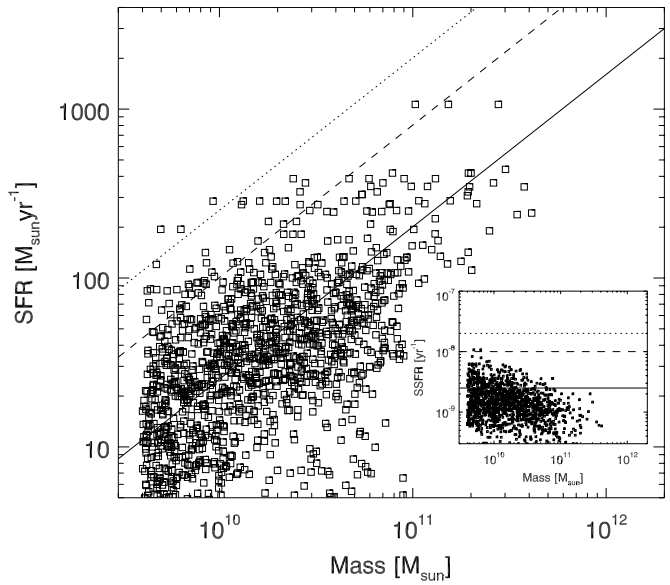

Figure 13. Star formation rates vs. stellar mass for the final model (squares) evaluated in the redshift interval $1.5 < z < 2.5$. The figure is formatted as for Figure 1 from Rodighiero et al. (2011) to facilitate comparison to that updated work on the measured SFR-mass distribution at $z \sim 2$. The solid line in the main plot shows the star-formation main sequence from Daddi et al. (2007), and the dashed and dotted lines are 4 and 10 times that relation (in SFR). As in Rodighiero et al. (2011) we also show the sSFR vs. mass relation for the same data in the inset plot; we use the same overplotted lines as in that paper (these are *not* exactly the main sequence line and multiples shown in the main plot).

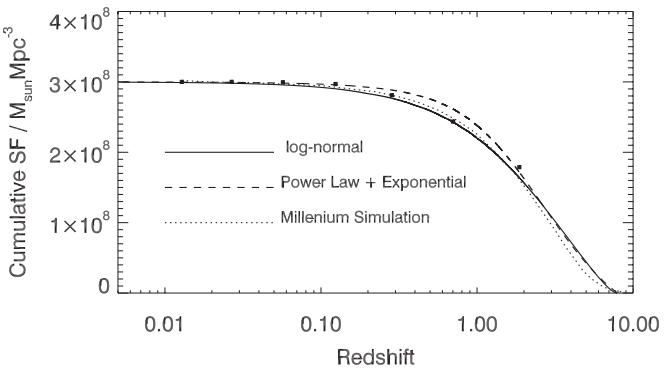

Figure 14. The cumulative star formation vs. redshift diagram from Panter et al. (2007). Solid points show their measurements, and their scaled version of the predicted measurement from Croton et al. (2006) is shown as a dotted line. The solid line shows the best fit log-normal to these cumulative data, and the dashed line is the best fit power law + exponential. The best fit log-normal is given by $t_0 = 1.564$ and $\tau = 1.728$.

which the rise time and peak time are described by a single parameter).

To further explore this question, we next consider a model constructed identically to that in Section 2.2, except that the log-normal SFH for each galaxy is replaced with a Gaussian SFH. This model has the same number of degrees of freedom as the log-normal model discussed in Section 3.1. As before, the ensemble of 2094 $z \sim 0$ galaxies is fit jointly with the cosmic SFRD, producing a realization that matches both of these constraints. As in Section 3.1 we then compute the model sSFR distributions in the higher redshift intervals and compare to the measured data; the comparison is shown in Figure 12, with identical scaling as Figure 7 to facilitate comparison. The lack of agreement achieved by this Gaussian SFH is striking—it clearly does not describe the higher redshift galaxy population with any significant fidelity, completely unlike the log-normal model. This implies that it is not simply that the log-normal model contains two independent parameters that provides the agreement seen in Figure 7, but rather that the functional form is itself important.

As a further illustration of the efficacy of the log-normal SFH in describing most galaxies, consider Figure 13. This shows the computed star formation rate versus stellar mass for the final model from Section 3.2, but now evaluated over the redshift interval $1.5 < z < 2.5$. Our aim here is to compare to the $z \sim 2$ star forming main-sequence from Daddi et al. (2007); the figure is formatted as for Figure 1 from Rodighiero et al. (2011) to facilitate comparison to that updated work. As in Section 3.1 we draw a redshift of evaluation for each $z \sim 0$ galaxy from the higher redshift interval considered; lacking detailed information about the high-sample we draw redshifts with equal probability from that interval. Also as in Section 3.1 we have computed the effect of mergers using merger rates from Xu et al. (2012); in this particular application we allow mergers up to three deep into the merger tree, so that any one $z \sim 0$ galaxy can be broken into up to eight components in the higher-z bin. As before, we do not attempt to compute individual histories for each component; all un-merged pieces of a $z \sim 0$ galaxy have the same SFH. Nevertheless, the model data shown in Figure 13 are a reasonable match to the $z \sim 2$ star-forming main sequence of Daddi et al. (2007)—despite no direct constraint being applied to the model at these redshifts apart from the integrated cosmic SFRD constraint. The fidelity with which this model can reproduce this higher redshift data on star formation, when constrained in detail only at lower redshifts, argues again that the underlying log-normal SFHs are a close approximation to the actual SFHs of individual galaxies.

Detailed analyses of the shape of SFH of galaxies, at both high and low redshifts, from both observational data and theoretical modeling, can also be described by a log-normal. For example, the recent literature includes archeological efforts to measure the SFH of local galaxies by resolved color–magnitude diagrams of their stellar populations (e.g., Williams et al. 2011; Dolphin 2002). In a larger but still reasonably local volume Panter et al. (2007) have analyzed the SFH of galaxies taken from the SDSS by a careful comparison of spectra to spectral synthesis models. The aggregate analyses (Panter et al. 2007; Williams et al. 2011) effectively reproduce an SFRD that looks similar to the data used in Figure 1 and elsewhere and so presumably can be fit by a log-normal; interestingly the analysis of Williams et al. (2011) sees the same elevated local SFRD from very low-mass galaxies that we were forced to include in Section 2.2. In Figure 14 we show a log-normal fit to the measured cumulative star formation from Panter et al. (2007); the fit is excellent. This fit is distinct from the fit presented in Figure 1, but of similar overall shape. Our goal here is not argue the exact match or lack thereof between the analysis of Panter et al. (2007) and direct in situ measurements of the cosmic SFRD but simply to note that the SFH suggested by those independent local data can indeed also be well fit by a log-normal SFH. For comparison Figure 14 also shows a fit using the power law + exponential form of Behroozi et al. (2013)—as in the fit to the cosmic SFRD (cf. Figure 1) this functional form is a reasonable description of the data, though it provides a poorer fit than a single log-normal.

At redshifts earlier than the peak in the cosmic SFRD Papovich et al. (2011) present the SFH of galaxies with a fixed comoving number density of 2×10^{-4} Mpc^{-3} and show that their SFR rises with time; they argue for a power-law description

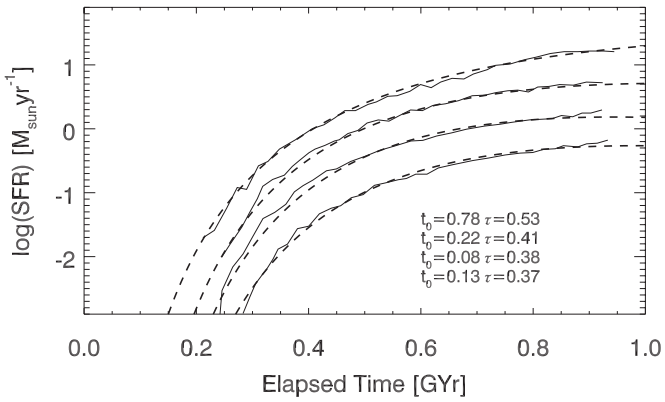

Figure 15. The simulated mean SFH of galaxies in the early universe ($z > 5.5$) from (Finlator et al. 2011; solid lines) in mass bins centered, from top to bottom, at masses of $\log M_*/M_\odot = 9.7, 9.2, 8.7,$ and 8.2. The dashed lines show the best-fitting log-normal function to each of these mean SFHs.

of the SHF of these galaxies over the interval $3 < z < 8$, although they note that an inverted-τ model is statistically indistinguishable from the power-law fit. We have fit the SFH data from Papovich et al. (2011) using a log-normal SFH in addition and find that it is also statistically indistinguishable from a power law as well (and is formally a better fit).

Finally, Figure 15 shows one further illustration of the utility of the log-normal SFH. We have fit the mean SHFs derived from cosmological hydrodynamic simulations in Figure 1 of Finlator et al. (2011) using log-normals. The rising mean SFHs for each mass bin from Finlator et al. are extremely well described by a log-normal function in each case.

6. FUTURE WORK AND CONCLUSIONS

The modeling effort presented above can be significantly expanded in several ways. Though we defer such work to further papers, we note here for reference some future tests which may be applied to the log-normal SFH framework that we have proposed.

1. *The computation of spectrophotometric properties across galaxy type and redshift.* Such calculations were one of the main drivers for the development of stellar population modeling. For example, the simplest measure (broadband galaxy colors) are strongly correlated to sSFRs; absent dust, colors are driven by the bluer light of the current star formation overlaid on the redder light of the SFH. The mapping between observed color and star formation rate is however non-linear, and instantaneous changes in the star formation rate of a given galaxy take several gigayears to be fully expressed in the galaxy's colors, and so a comparison of predicted and observed color distributions may provide additional model constraints, and may indicate the prevalence of processes outside the star formation regime considered here (e.g., rapid changes—bursts or truncations—in the SFH of individual galaxies).
2. *The apparent plateau in the sSFRs of galaxies at redshifts beyond $z \sim 2$.* Comparing models to observed galaxies will require a more robust treatment of mergers than we have used in this initial paper, since the strong relation between sSFR and mass in galaxy populations requires that models and data are compared over precisely the same mass range. The model proposed here may have the appropriate properties to produce the observed trend, however; in the model realizations above most galaxies at times earlier than the peak of the cosmic SFRD have smoothly increasing SFHs and will not have the extremely high sSFRs one would expect from alternate models which start at a high SFR and then decline (such as a declining τ model with a delayed start).

We also envision a further refinement to the model—simply that of modeling each galaxy as a pair of log-normal distributions, with an adjustable weight between the two components. Such a complication is motivated by the typical morphological structure of most galaxies, with an old spheroidal component, and a disky component with a more extend SFH. Though this would more than double the number of adjustable parameters in the resulting model realizations, it would also allow for additional constraints to be brought to bear. For example by requiring that one of the two components have an sSFR at the current epoch that is essentially zero (i.e., has an SFH appropriate for the spheroidal component of a galaxy, but with a varying weight set by the model) the model would produce (and could be constrained by) measurements of the bulge/disk ratio in galaxies.

Regardless, the efficacy with which log-normal SFHs reproduce the ensemble sSFRs of observed galaxies across a broad range of redshift and mass, and the utility of the log-normal form in describing the SFHs of a number of specific observed and simulated galaxy populations, demonstrates that at minimum these SFHs are a useful addition to the stellar population modeling toolkit. Moreover, the apparent ability of log-normal SFHs to predict the sSFR distributions of distant galaxies from only sSFR data at lower redshifts, coupled to the integral constraint of the cosmic SFRD, suggests a deeper significance—namely that the log normal SFH is a close approximation to the actual SFHs of most galaxies. This conclusion is strengthened by the inability of a normal (rather than log-normal) SFH model to reproduce the sSFR data; the shape of the distribution matters. Individual galaxies aside, the simple conclusion that the cosmic SFRD is lognormal in time seems to have not been previously recognized, and likely has a physical significance.

Finally, given the overall success of the log-normal SFH modeling, this paper provides further support to several of the conclusions of Paper III, namely that some galaxies, even at intermediate redshifts, are surprisingly young, and that the enhanced sSFRs of these objects are not due primarily to starbursts. The model realizations above show that the sSFR distributions to $z = 1$ can be fit with SFHs that are only smoothly varying, completely absent any bursting component.

M.D.G. thanks the Research Corporation for support of this work through a Cottrell Scholars award. We thank an anonymous referee for two rigorous and eminently helpful readings of the manuscript; their effort and advice improved the final paper significantly.

REFERENCES

Behroozi, P. S., Wechsler, R. H., & Conroy, C. 2013, ApJ, 770, 57
Bell, E. F., & de Jong, R. S. 2001, ApJ, 550, 212
Bouwens, R. J., Illingworth, G. D., Franx, M., et al. 2009, ApJ, 705, 936
Calvi, R., Poggianti, B. M., & Vulcani, B. 2011, MNRAS, 416, 727
Cimatti, A., Cassata, P., Pozzetti, L., et al. 2008, A&A, 482, 21
Cowie, L. L., Songaila, A., Hu, E. M., & Cohen, J. G. 1996, AJ, 112, 839
Croton, D. J., Springel, V., White, S. D. M., et al. 2006, MNRAS, 365, 11
Cucciati, O., Tresse, L., Ilbert, O., et al. 2012, A&A, 539, A31
Daddi, E., Dickinson, M., Morrison, G., et al. 2007, ApJ, 670, 156
Davis, M., Guhathakurta, P., Konidaris, N. P., et al. 2007, ApJL, 660, L1
de Barros, S., Schaerer, D., & Stark, D. P. 2012, arXiv:1207.3663

Di Matteo, P., Bournaud, F., Martig, M., et al. 2008, A&A, 492, 31
Dolphin, A. E. 2002, MNRAS, 332, 91
Finlator, K., Oppenheimer, B. D., & Davé, R. 2011, MNRAS, 410, 1703
Gavazzi, G., Bonfanti, C., Sanvito, G., Boselli, A., & Scodeggio, M. 2002, ApJ, 576, 135
González, V., Labbé, I., Bouwens, R. J., et al. 2010, ApJ, 713, 115
Jaacks, J., Nagamine, K., & Choi, J. H. 2012, MNRAS, 427, 403
Jungwiert, B., Combes, F., & Palouš, J. 2001, A&A, 376, 85
Kaviraj, S., Peirani, S., Khochfar, S., Silk, J., & Kay, S. 2009, MNRAS, 394, 1713
Kondo, K. 1977, Japan. J. Hum. Genetics, 21, 217
Larson, D., Dunkley, J., Hinshaw, G., et al. 2011, ApJS, 192, 16
Larson, R. B., & Tinsley, B. M. 1978, ApJ, 219, 46
Limpert, E., Stahel, W. A., & Abbt, M. 2001, BioSc, 51, 5
Maraston, C., Pforr, J., Renzini, A., et al. 2010, MNRAS, 407, 830
Noeske, K. G., Weiner, B. J., Faber, S. M., et al. 2007, ApJL, 660, L43
Oemler, A., Jr., Dressler, A., Gladders, M. G., et al. 2013a, ApJ, 770, 61 (Paper I)
Oemler, A., Jr., Dressler, A., Gladders, M. G., et al. 2013b, ApJ, 770, 63 (Paper III)
Panter, B., Jimenez, R., Heavens, A. F., & Charlot, S. 2007, MNRAS, 378, 1550
Papovich, C., Finkelstein, S. L., Ferguson, H. C., Lotz, J. M., & Giavalisco, M. 2011, MNRAS, 412, 1123
Reddy, N. A., Pettini, M., Steidel, C. C., et al. 2012, ApJ, 754, 25
Reddy, N. A., & Steidel, C. C. 2009, ApJ, 692, 778
Rodighiero, G., Daddi, E., Baronchelli, I., et al. 2011, ApJL, 739, L40
Salemi, S., Yang, L., Dai, J., Qin, J., & Bernstein, J. B. 2008, Physics-of-Failure Based Handbook of Microelectronic Systems (Utica, NY: Reliability Information Analysis Center)
Sandage, A. 1986, A&A, 161, 89
Searle, L., Sargent, W. L. W., & Bagnuolo, W. G. 1973, ApJ, 179, 427
Stark, D. P., Ellis, R. S., Bunker, A., et al. 2009, ApJ, 697, 1493
van der Burg, R. F. J., Hildebrandt, H., & Erben, T. 2010, A&A, 523, A74
Williams, B. F., Dalcanton, J. J., Johnson, L. C., et al. 2011, ApJL, 734, L22
Wyder, T. K., Treyer, M. A., Milliard, B., et al. 2005, ApJL, 619, L15
Xu, C. K., Zhao, Y., Scoville, N., et al. 2012, ApJ, 747, 85